Four years of operation of the Chandra X−ray Observatory

Martin C. Weisskopf

Space Science Department, NASA/Marshall Space Flight Center

ABSTRACT

The on−orbit performance of the Chandra X−Ray Observatory over its first four years of operation is reviewed. The Observatory is running smoothly and the scientific return continues to be superb.

Keywords: x−ray imaging, grazing−incidence optics, x−ray astronomy.

1. INTRODUCTION

The Chandra X−Ray Observatory is the X−ray component of NASA's Great Observatory Program. The facility provides scientific data to the international astronomical community in response to proposals for its use. Data becomes public at most one year after the observation. The Observatory is the product of the efforts of many commercial, academic, and government organizations in the United States and Europe. NASA's Marshall Space Flight Center (MSFC) manages the Project and provides Project Science; NGST (formerly TRW) served as prime contractor responsible for providing the spacecraft, the telescope, and assembling and testing the observatory; and the Smithsonian Astrophysical Observatory (SAO) provides technical support and is responsible for ground operations including the Chandra X−Ray Center (CXC).

2. THE OBSERVATORY

In 1977, NASA/MSFC and SAO began the study leading to the definition of the then named Advanced X−Ray Astrophysics Facility mission. This study, in turn, had been initiated as a result of an unsolicited proposal submitted to NASA in 1976 by Prof. R. Giacconi (Harvard University and SAO) and Dr. H. Tananbaum (SAO). Several significant events took place during the intervening years including the highest recommendation by the National Academy of Sciences Astronomy Survey Committee, selection of the instruments, selection of the prime contractor, demonstration of the ability to build the optics, restructuring of the mission, selecting the name of the mission in honor of the Nobel Prize winner Subramanyan Chandrasekhar, and the launch. This past year, Prof. Giacconi was awarded the Nobel Prize for his pioneering work in X−ray astronomy.

The launch took place on July 23, 1999 using the Space Shuttle Columbia. The Commander was Col. Eileen Collins, the first female commander of a Shuttle flight. With a second rocket system, the Inertial Upper Stage (IUS) attached, the Observatory was both the largest and heaviest payload ever launched by and deployed from a Space Shuttle. Once deployed, and after separating from the IUS, the flight system illustrated in Figure 1 is 13.8−m (43.5−ft) long by 4.2−m (14−ft) diameter, with a 19.5−m (64−ft) solar−panel wingspan. With extensive use of graphite−epoxy structures, the mass is 4,800 kg (10,600 pounds).

The IUS performed two firings and separated from the Observatory. Finally, after five firings of the internal propulsion system − the last of which took place 15 days after launch − the Observatory was placed in its highly elliptical orbit. This orbit has a nominal apogee of 140,000 km and a nominal perigee of 10,000 km. The inclination to the equator is 28.5°. The satellite is above the radiation belts for more than 75% of the 63.5−hour orbital period.

The spacecraft is standard except for its lightweight construction and provides pointing control, power, command and data management, thermal control, and other such services to the scientific payload. The principal elements of the payload are the x−ray telescope, the scientific instruments, and the aspect system used to determine where the observatory was pointed.

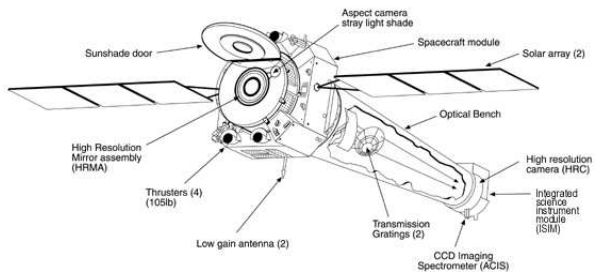

Figure 1. The Chandra X−Ray Observatory.

The specified design life of the mission is 5 years; however, the only perishable (gas for maneuvering) is sized to allow operation for more than 10 years. NASA has recently officially recognized a 10−year mission. The orbit will be stable for decades.

3. USEAGE AND EFFICIENCY

The observing efficiency is dominated by the time spent in the radiation belts at altitudes below about 60,000 km. Other impacts are solar activity, maneuver time, etc. Figure 2 summarizes one year of operations.

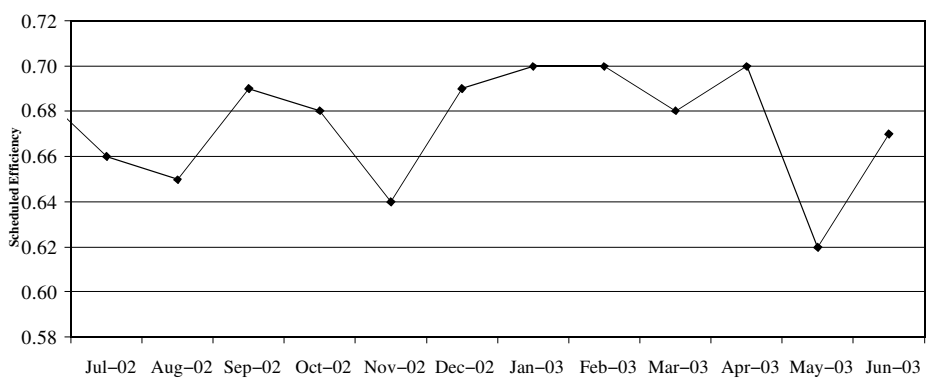

Figure 2. Observing efficiency (time on target) for one year of operation.

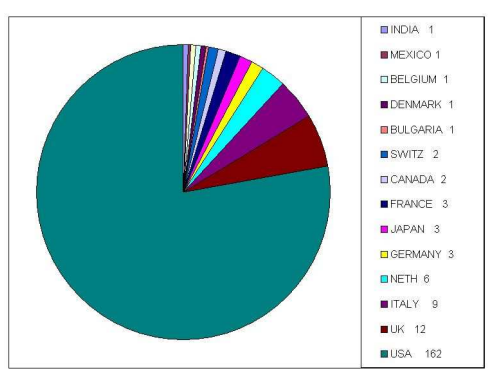

Figure3. Country of origin of the Chandra Principal Investigators for observing cycle 5.

The CXC has recently completed the review of proposals in response to the fifth announcement of opportunity. There were 785 proposals with Principal Investigators from 21 countries. These included 14 Very Large Projects (those that require more than 1000 ksec to perform), 54 Large Projects (those that require 300 ksec or more), 71 proposals to use the Chandra archives, and 40 proposals to perform theoretical research that has direct impact on the analysis and interpretation of Chandra data. The peer review accepted 208 observing proposals of which 3 were very large projects, 7 were large projects. In addition, 17 archive and 18 theory proposals were accepted. Figure 3 illustrates the distribution of the country of the Principal Investigator.

4. INSTRUMENTATION

The first x−rays focused by the telescope were observed on August 12, 1999. Figure 4 shows one of the early images. This image of the Crab Nebula and its pulsar included a new discovery − the bright inner elliptical ring showing the first direct observation of the shock front where the wind of particles from the pulsar begins to radiate in x−rays via the synchrotron process. Discoveries of new astronomical features in Chandra images have been the rule, not the exception.

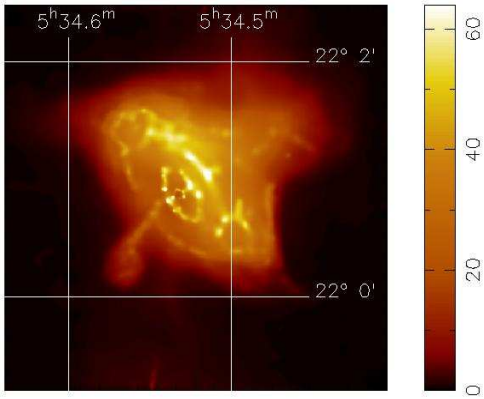

Figure 4. Chandra image of the Crab Nebula

The Chandra optics and detectors provide, for the first time, sub−arcsecond imaging, sub−arcsecond spectrometric imaging, and, together with transmission gratings, high−resolution x−ray spectroscopy. With these capabilities, a wide variety of high−energy phenomena in a broad range of astronomical objects are being observed. The telescope is made of four concentric, precision−figured, superpolished Wolter−1 x−ray telescopes, similar to those used for both the Einstein and Rosat observatories, but of much higher quality, larger diameter, and longer focal length. The Wolter−1 design uses a paraboloid of revolution followed by a hyperboloid of revolution. Two reflections minimize coma. The 4−mirror−pair grazing−incidence optic is constructed of Zerodur, a glassy ceramic chosen for its high thermal stability. The mirrors are coated with iridium, chosen for high reflectivity at the x−ray energies of interest, 0.08 − 10.0−keV (15−0.12 nm).

The aspect camera system includes a visible−light telescope and CCD camera attached to the x−ray telescope. A fiducial−light transfer system is used to project lights attached to the focal−plane instruments onto the aspect camera. Thus, the aspect camera simultaneously determines both where the observatory was pointing and the location of the x−ray detector positions relative to the pointing direction. The aspect solution's accuracy depends on the number of stars detected in the field, but is typically 0.6 seconds of arc.

The science instrument module includes mechanisms for focusing and translating the focal−plane instruments. Translation of the instruments is required as x−ray beam−splitters are not very efficient.

Just behind the telescope are 2 objective transmission gratings − the Low−Energy Transmission Grating[1] (LETG), optimized for longer x−ray wavelengths and the High−Energy Transmission Grating[2] (HETG), optimized for shorter wavelengths. Positioning mechanisms may insert either grating into the converging beam to disperse the x−radiation

onto the focal plane producing high−resolution spectra read−out by one of the detectors. Figure 5 illustrates the concept for the HETG. The LETG is similar except that all the facets are identical. The gratings allow for measurements with spectral resolving power of $\lambda/\Delta\lambda = E/\Delta E > 500$ for wavelengths of > 0.4−nm (energies < 3 keV).

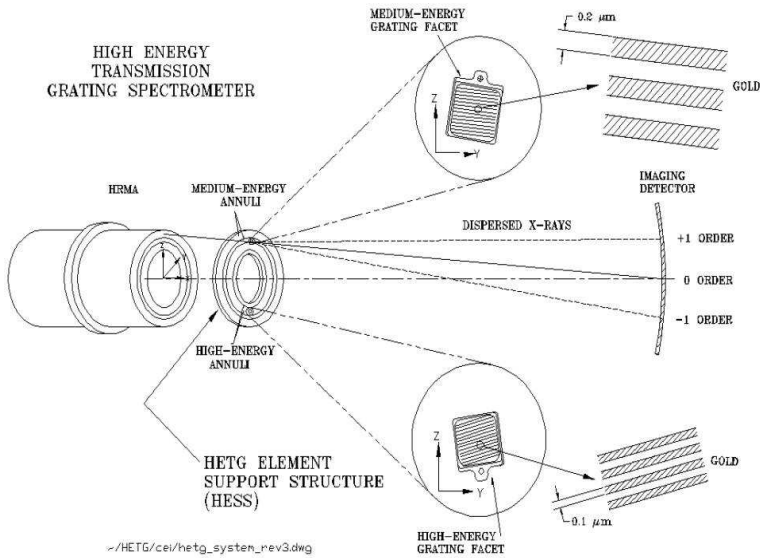

Figure 5. Grating layout.

The Space Research Institute of the Netherlands and the Max−Planck−Institut fur Extraterrestrische Physik designed and fabricated the LETG. The assembly is made of 540 grating facets with gold bars of 991−nm period. The LETG provides high−resolution spectroscopy from 0.08 to 2 keV (15 to 0.6 nm).

The Massachusetts Institute of Technology (MIT) designed and fabricated the High−Energy Transmission Grating (HETG). The HETG uses 2 types of grating facets − the Medium−Energy Gratings (MEG) which, when inserted, are placed behind the telescope's 2 outermost shells, and the High−Energy Gratings (HEG), behind the 2 innermost shells. The HEG and MEG are oriented at slightly different dispersion directions. With polyimide−supported gold bars of 400−nm and 200−nm periods, the HETG provides high−resolution spectroscopy from 0.4 to 4 keV (MEG, 3 to 0.3 nm) and from 0.8 to 8 keV (HEG, 1.5 to 0.15 nm).

Chandra's two focal−plane science instruments are the High Resolution Camera[3] (HRC) and the Advanced CCD Imaging Spectrometer (ACIS)[4].

SAO designed and fabricated the HRC. One of the HRC detectors is made of a 10−cm−square microchannel plate, and provides high−resolution imaging over a 31−arcmin−square field of view. A second detector, comprising 3 rectangular segments (3−cm−by−10−cm each) mounted end−to−end along the grating dispersion direction, serves as the primary read−out detector for the LETG. Both of the HRC detectors are coated with a cesium−iodide photocathode and have thin aluminized polyimide shields to prevent contamination by ions and ultraviolet light.

The Pennsylvania State University MIT built the Advanced CCD Imaging System (ACIS) with charge−coupled devices (CCDs) fabricated by MIT's Lincoln Laboratory. As with the HRC, there are two detector systems. One is made of a 2−by−2 array of CCDs, and provides high−resolution spectrometric imaging over a 17−arcmin−square field of view. The other, a 6−by−1 array mounted along the grating dispersion direction, serves as the primary read−out detector for the HETG. Two types of CCDs were used, 8 front−illuminated (FI) and two back−illuminated (BI). The latter CCDs have higher efficiency at lower energies than the FI devices, but were much more difficult to fabricate. One BI CCD was placed at the on−axis focal position of the 6 x 1 array. Thus this particular CCD also provides high−resolution spectrometric imaging extending to lower energies, but over a smaller (8−arcmin−square) field than the 2 x

2 array. Both ACIS detector systems have thin aluminized polyimide filters to minimize contamination by visible light.

Despite successful science operations, the Observatory has had to deal with a number of technical difficulties that have had their impact on scientific performance. The front− (not the back−) illuminated ACIS CCDs suffered damage, which increased the charge transfer inefficiency as a result of bombardment by low energy (100 keV) protons crudely focused by the telescope by means of Rutherford scattering as the Observatory entered the radiation belts. Following a procedure of removing ACIS from the focal plane during radiation belt passages has dramatically minimized subsequent increases in the charge transfer inefficiency. O'Dell et al.[5] discuss the Chandra approach to radiation management.

Both ACIS filters, which are close to the coldest (120 °C) surfaces on the observatory, are collecting hydrocarbon contamination at the rate of about one−half an optical depth at the Carbon k−edge per year. Figure 6 illustrates the contamination build up based on two different methods of quantifying the impact based on our current understanding of the chemical composition and rate of deposition of the contaminants. Marshall et al. discuss the composition of the contaminant in more detail in these proceedings. Normally, we would plan to bake off the contamination. Bake out is, however, complicated, by the potential impact on the charge transfer efficiency of the CCDs. A bake out strategy that involves a minimum temperature increase is being developed.

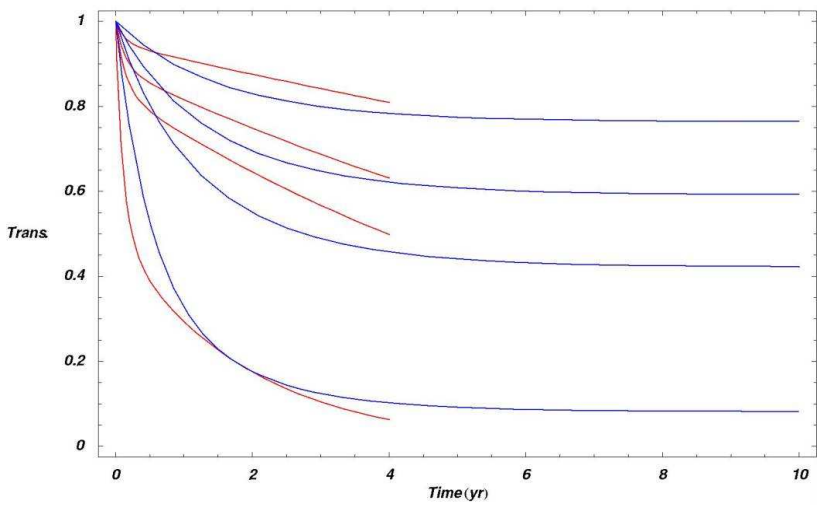

Figure 6. Transmission of the contaminant on the ACIS for different energies (0.9, 0.7, 0.5, and 0.3 keV top to bottom) versus time since launch in years for two different contamination models. The curves that extend beyond the present is for the ACISABS model with default parameters. This model is available to CIAO and XSPEC users. Marshall et al. discuss the second model in these proceedings

Point Spread Function

The Observatory's point spread function, as measured during ground calibration, had a full width at half−maximum less than 0.5 arcsec and a half−power diameter less than 1 arcsec. The pre−launch prediction for the on−orbit encircled−energy fraction was that a 1−arcsec−diameter circle would enclose at least half the flux from a point source. A relatively mild dependence on energy, resulting from diffractive scattering by surface microroughness, attest to the 3 angstroms rms surface roughness The ground measurements were, of course, taken under environmental conditions quite different than those encountered on−orbit. The effects of gravity on the optics and the finite distance and the size of the various x−ray sources used were of course unique to the ground calibration. On−orbit the performance includes the spatial resolution of the flight detectors and any uncertainties in the aspect solution. The on−orbit performance met expectations as illustrated in Figure 7.

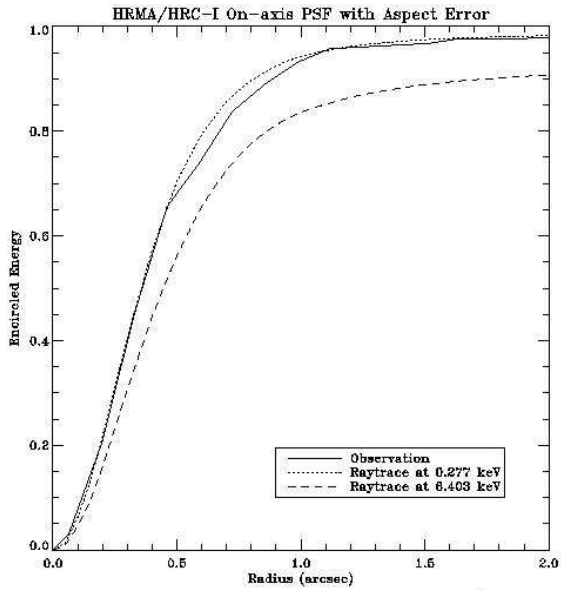

Figure 7. Encircled energy versus radius comparing pre−launch predictions at two energies to on−orbit performance.

The tremendous advancement in angular resolution that the Chandra optics provides, introduces new considerations for the analysis of the data. An example is that now one has to account for the energy dependence of the flux scattered out of the beam by the interstellar medium.

The Observatory's capability for high−resolution imaging enables detailed high−resolution studies of the structure of extended x−ray sources, including supernova remnants, astrophysical jets, and hot gas in galaxies and clusters of galaxies. The additional capability for spectrometric imaging allows studies of structure, not only in x−ray intensity, but also in temperature and in chemical composition. Through these observations, users are addressing several of the most exciting topics in contemporary astrophysics.

In addition to mapping the structure of extended sources, the high angular resolution permits studies of discrete sources, which would otherwise be impossible. In example is shown in Figure 8 where one sees x−rays produced by TWA 5B, a brown dwarf orbiting a young binary star system known as TWA 5A[6]. This observation is important not only in demonstrating the angular resolution but for addressing the question as to how do brown dwarfs heat their upper atmospheres, or coronas, to x−ray−emitting temperatures of a few million degrees.

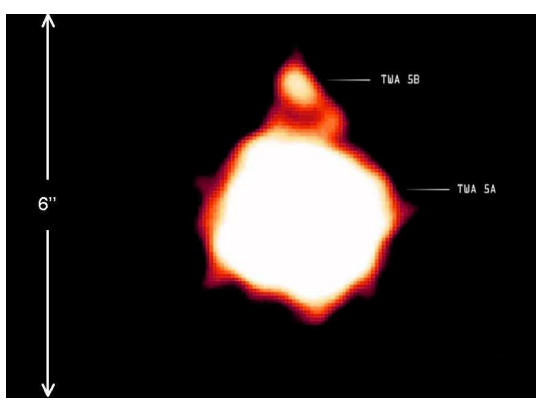

Figure 8. X−rays produced by TWA 5B, a brown dwarf orbiting a young binary star system known as TWA 5A. Courtesy of NASA/CXC/Chuo U[7]

Equally important are Chandra's unique contributions to high−resolution dispersive spectroscopy. As the capability for visible−light spectroscopy initiated the field of astrophysics about a century ago, high−resolution x−ray spectroscopy now contributes profoundly to the understanding of the physical processes in cosmic x−ray sources and is the essential tool for diagnosing conditions in hot plasmas. The high spectral resolution of the Chandra gratings isolates individual lines from the myriad of spectral lines, which would overlap at lower resolution.

5. DISCOVERIES

From planetary systems to deep surveys of the faintest and most distant objects, the scientific results from the first four years of Chandra operations have been exciting and outstanding. We conclude this overview with a series of images illustrating some these results with more emphasis on results obtained this past year. We begin with images of the x−ray emission from the planet Jupiter. Figure 9 shows hot spots at high (and unexpected) latitudes that appear to pulsate at approximately a 45−minute period.[8] In this case the x−rays appear to be produced by particles bombarding the Jovian atmosphere after precipitating along magnetic field lines. Figure 10 continues the discoveries about the Jovian system and shows the first detection of x−rays from two of the moons.[9] In Figure 11 we show the more recent detection[10] of fluorescent scattering of solar X−rays in the upper Mars atmosphere. The X−ray spectrum is dominated by a single narrow emission line, which is most likely caused by O−K fluorescence.[11]

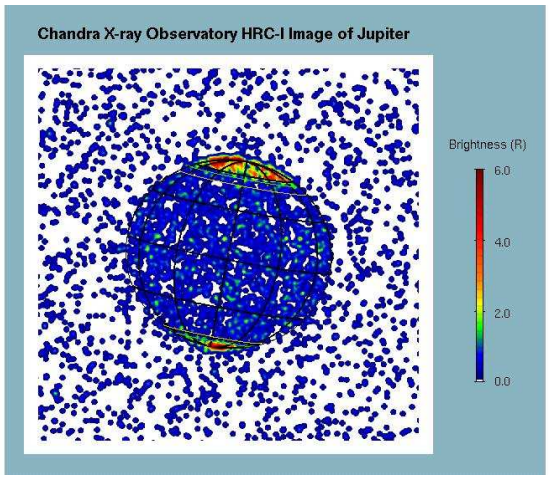

Figure 9. Chandra image of the x−ray emission from Jupiter. Courtesy of R. Elsner.

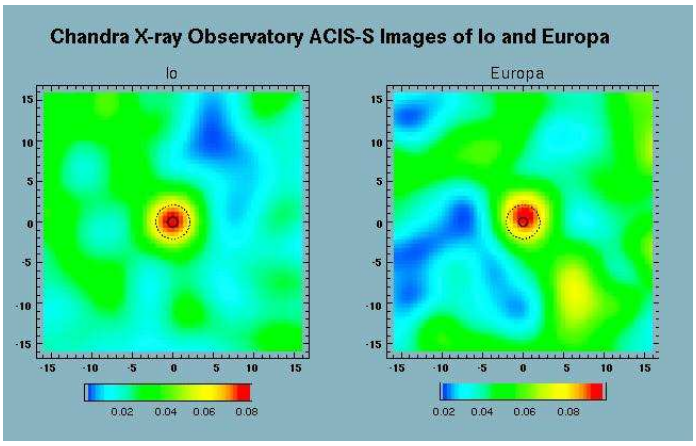

Figure 10. Chandra HRC image of x−rays from the Jovian moons Io and Europa. Courtesy of R. Elsner.

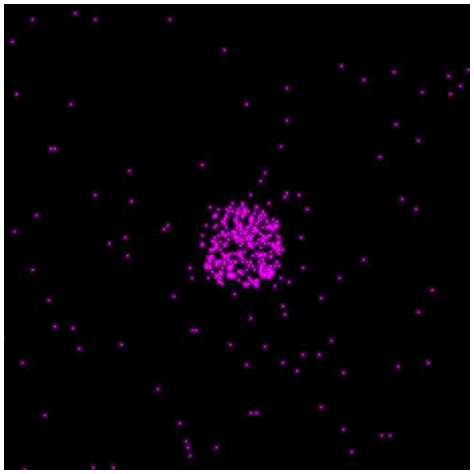

Figure 11. Chandra image of Mars. Image is 2 arcmin on a side and the Mars disk is 20.3 arcsec in diameter. Courtesy NASA/CXC/MPE/K.Dennerl et al.

One of the most spectacular Chandra images is the one of the center of our own galaxy[12] shown in Figure 12. Here we clearly see the presence of both point−like discrete sources (over 1000) and diffuse extended emission. The large amounts of hot gas has been heated and chemically enriched by numerous stellar explosions.

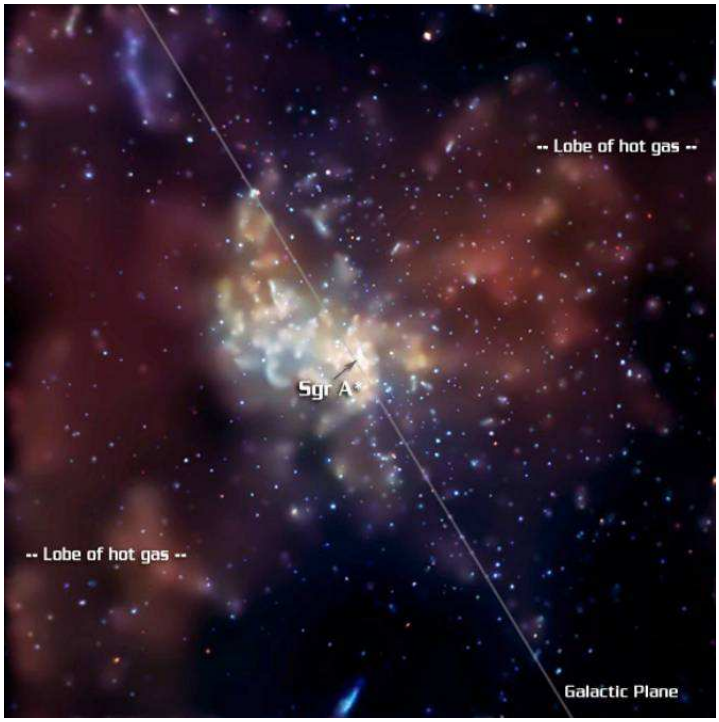

Figure 12.Chandra image of the Galactic Center. The image is 8.4 arcmin on a side. Courtesy NASA/CXC/MIT/F.K.Baganoff et al.

Figure 13 shows a time history and relative positioning of the optical emission of SNR 1987 A as seen with HST together with the x−ray emission observed with Chandra.[13]

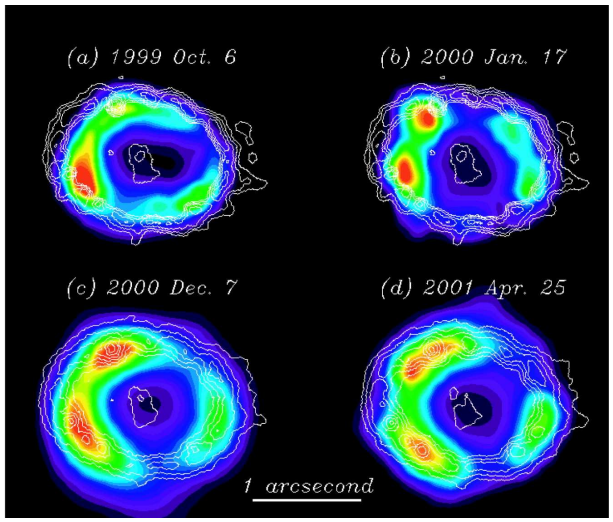

Figure 13. ACIS images and HST contours of the emission from SNR1987A. Courtesy Dave Burrows.

The final legacy of Chandra may ultimately be led by the spectroscopic data. The energy resolution, enabled by the quality of the optics, is providing new and extremely complex results. For example, high−resolution spectra of Seyfert galaxies are providing new details about the physical and dynamical properties of material surrounding the active nucleus. In the case of Seyfert 1s, whose signal is dominated by a bright X−ray continuum from the central engine, the partially ionized circum−source material introduces prominent patterns of absorption lines and edges. Figure 14, e.g. shows a LETG/HRC spectrum of NGC 5548. This spectrum has dozens of absorption lines.[14]

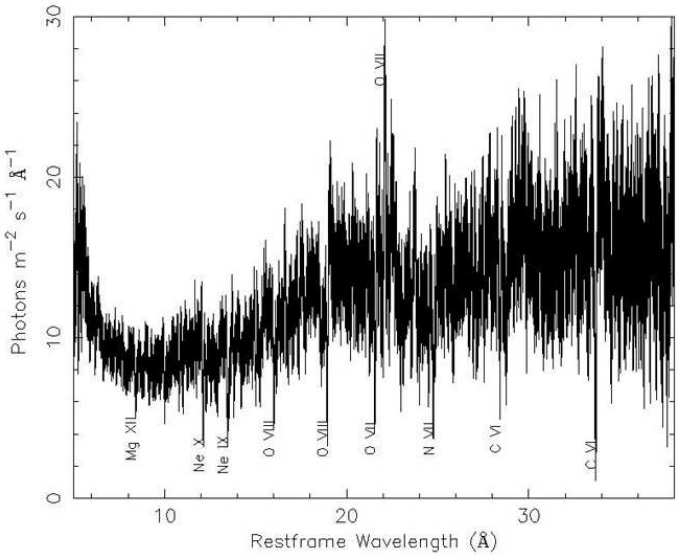

Figure 14. LETG/HRC spectrum of the Seyfert 1 galaxy NGC 5548.[14] Several prominent absorption lines from H−like and He−like ions are marked, as is the forbidden line of He−like oxygen.

For Seyfert 2's the strong continuum from the central engine is not seen directly, so the surrounding regions are seen in emission. Figure 15 provides an example of an LETG/HRC observation of NGC 1068.

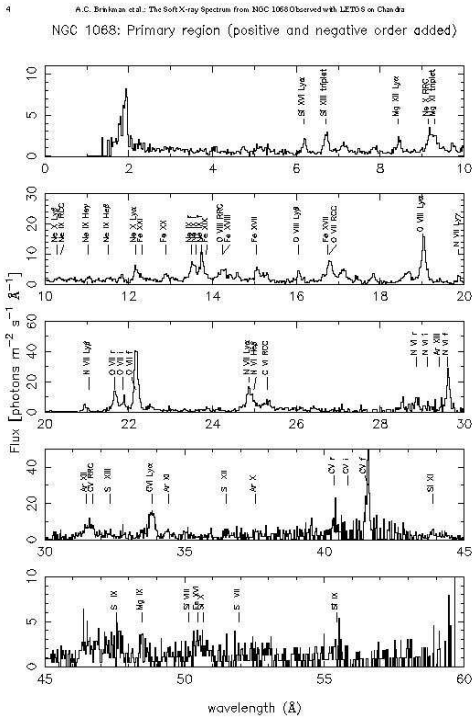

Figure 15. Emission−line spectrum from the Seyfert 2 galaxy NGC 1068.[15] Kindly provided by A. Kinkhabwala .

One of the more important triumphs of the Observatory has been to use the angular resolution and high sensitivity to perform detailed surveys of extended objects such as globular clusters, galaxies, and clusters of galaxies. Figure 16 shows one of the spectacular Chandra images of globular clusters.[16] A survey of two interacting galaxies is illustrated in Figure 17 where one sees emission from diffuse gas and bright point sources.

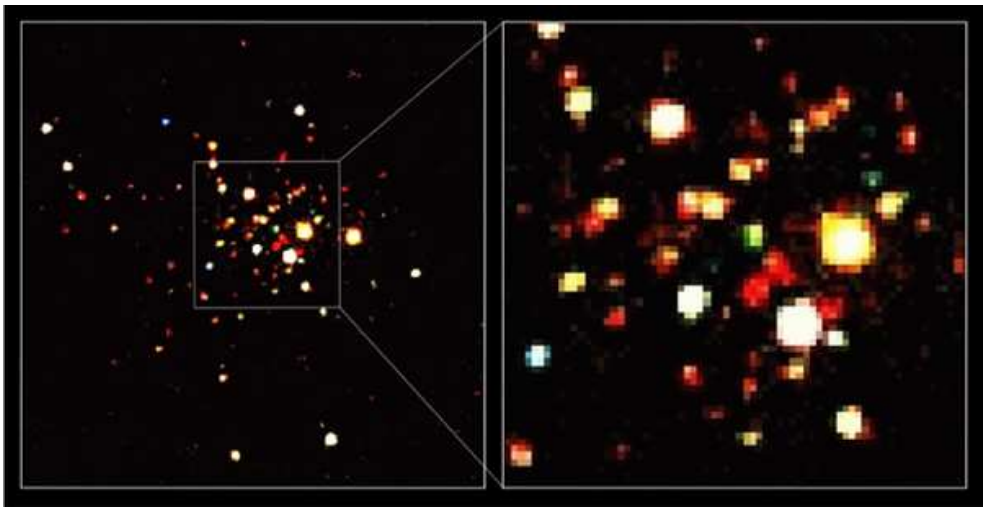

Figure 16. Chandra ACIS image of the globular cluster 47 Tucanae. The left panel covers the central 2' x 2.5'. The central 35" x 35" are shown to the right. Courtesy NASA/CfA/J.Grindlay et al.

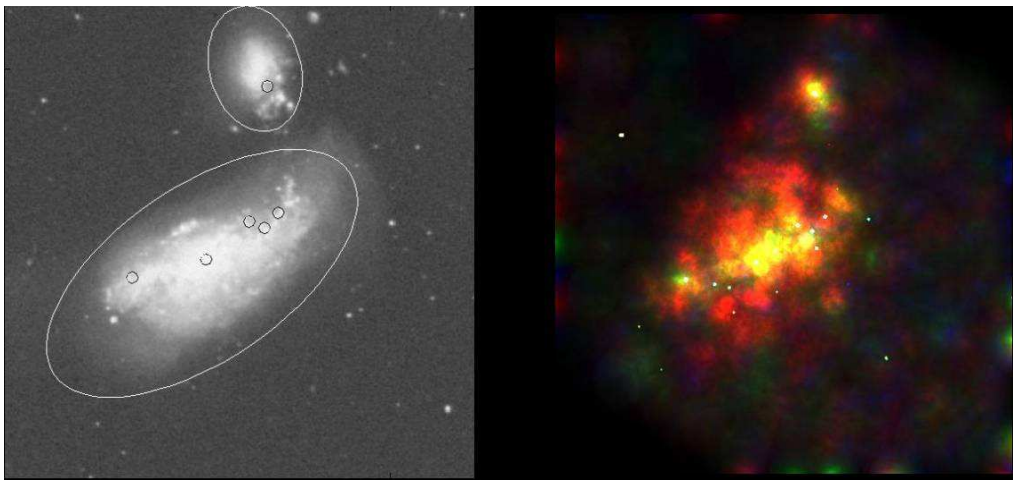

Figure 17. Optical (Digitized Sky Survey) image (left) and X−ray (Chandra) image (right) of two interacting galaxies NGC 4490 and 4485. Large ovals represent the approximate boundaries of the galaxies (NGC 4490 is the larger of the two). Small circles indicate the brightest X−ray sources. Courtesy Doug Swartz

.

Chandra observations of clusters of galaxies frequently exhibit previously undetected structures with characteristic angular scales of a few arc seconds. These include "bubbles" where there is strong radio emission, bow shocks, and cold fronts. These are illustrated in Figures 18,19, and 20. Figure 18 of the Perseus cluster[17] is a spectacular example of bubbles produced in regions where there is strong radio emission. Figure 19 shows a bow shock propagating in front of a bullet−like gas cloud just exiting the disrupted cluster core. This observation of the galaxy cluster 1E0657−56 is the first clear example of such a shock front.[18] In contrast, Figure 20 of Abell 2152[19] is an example of a shockless cold front. A major triumph of Chandra and XMM−Newton high−resolution spectroscopic observations has been the discovery that that gas in the clusters is typically not cooling to below about 1−2 keV.[20]

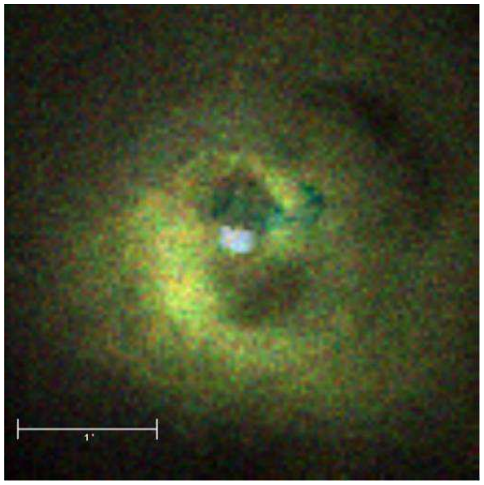

Figure 18. X−ray core of the Perseus cluster. Courtesy NASA/IoA/A. Fabian et al.

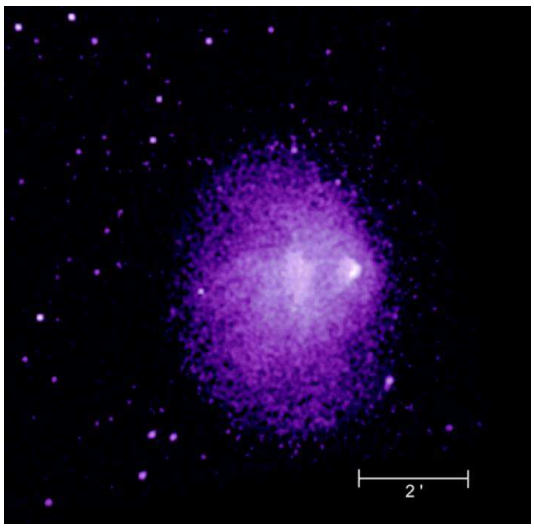

Figure 19. The Chandra image of the merging, hot galaxy cluster 1E 0657−56. Courtesy NASA/SAO/CXC/M.Markevitch et al.

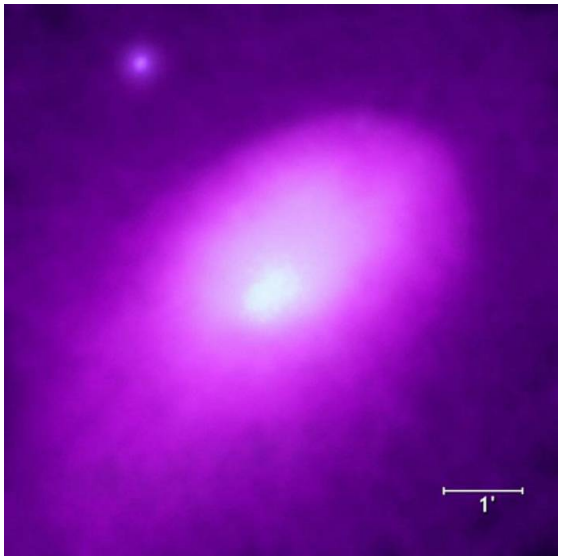

Figure 20. Chandra Image of the galaxy cluster Abell 2142. The sharp border to the top right is an example of a cold front. Courtesy NASA/CXC/SAO

Figure 21 illustrates multiwavelength observations of the jets from active galaxies. The Chandra x−ray image[21] shows an irregular, knotty structure similar to that seen at radio and optical[22] wavelengths. However, the knots near the central core are much brighter in X−rays

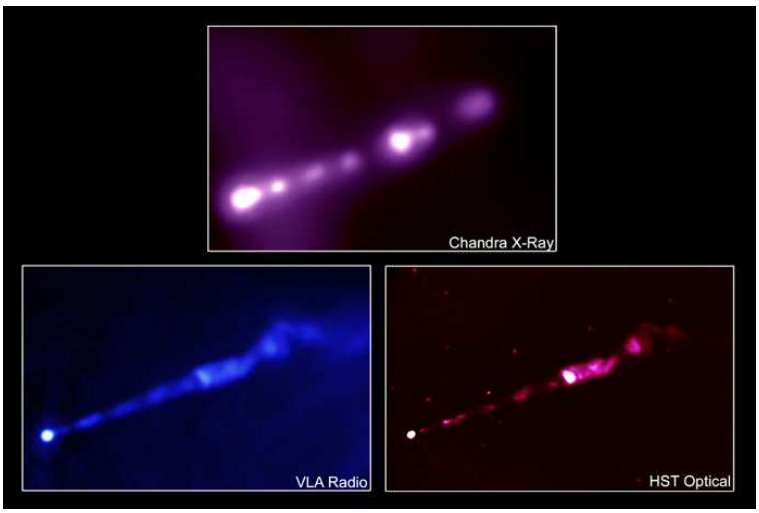

Figure 21. The x−ray jet emanating from the nucleus of the elliptical galaxy M87 as seen in three wavelength bands. Credits: X−ray: NASA/CXC/MIT/H. Marshall et al. Radio: F. Zhou, F.Owen (NRAO), J.Biretta (STScI) Optical: NASA/STScI/UMBC/E.Perlman et al.

The jet phenomenon is ubiquitous in astronomical settings, especially with regards to x−ray emission. One of the most spectacular recent Chandra discoveries has been the series of observations of the outer jet of the Vela pulsar[23] a few of which are illustrated in Figure 22.

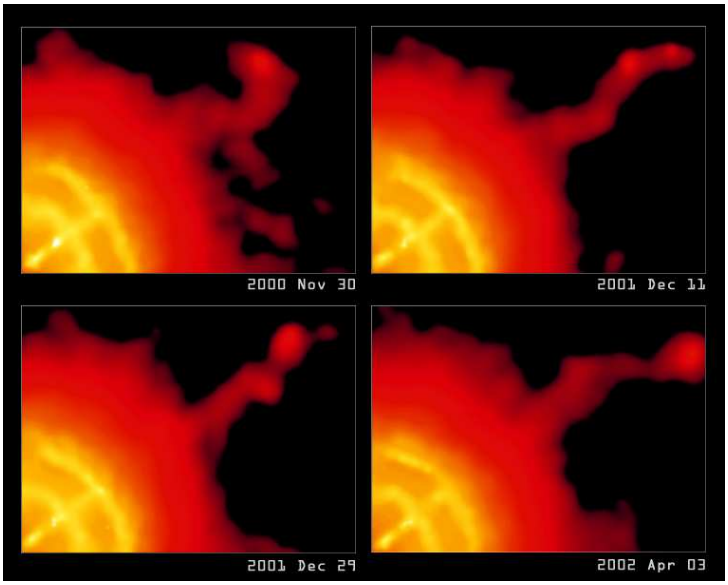

Figure 22. Four observations of the Vela Pulsar and its outer jet. Each image is 1.6 x 1.2 arcmin Courtesy NASA/CXC/PSU/G.Pavlov et al.

No discussion of data taken with the Observatory is complete without a mention of the deep Chandra Surveys. These are deep exposures of particular regions of the sky to study the populations of the objects detected, especially the faintest ones. This work is an outgrowth of the study the diffuse x−ray background, the nature of which had been a puzzle for nearly 40 years, although the lack of distortion of the spectrum of the Cosmic Microwave Background placed a strong upper limit to the possibility of a truly diffuse component[24] Observations with ROSAT at energies

below 2 keV made a major step in resolving a significant fraction (70−80%) into discrete objects.[25] Currently two long exposures have been accomplished with the Chandra X−Ray Observatory − the Chandra Deep Fields North[26] depicted in Figure 23 with 2 Ms of exposure, and the Chandra deep field south[27] with 1 Msec. These surveys have extended the study of the background to flux levels more than an order of magnitude fainter than previously in the 0.5−2.0 keV band and have resolved over 90% of the background into a variety of discrete sources. The largest uncertainty in establishing the fraction is now in the knowledge of the total level of the background itself.

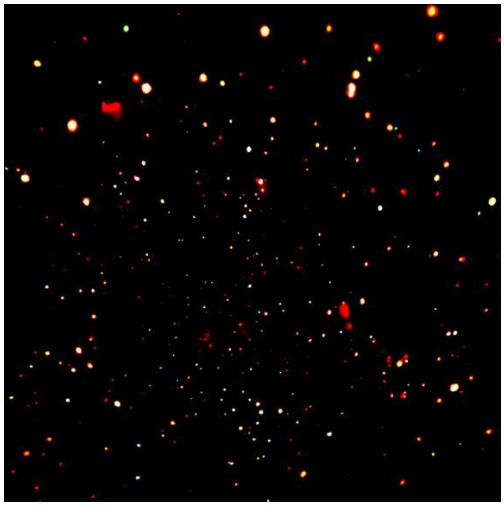

Figure 23. Two−million−second image of the Chandra Deep Field North. Courtesy NASA/CXC/PSU/D.M.Alexander, F.E.Bauer, W.N.Brandt et al.

6. WORLD−WIDE WEB SITES

The following lists several Chandra−related sites on the World−Wide Web

http://chandra.harvard.edu/: Chandra X−Ray Center (CXC), operated for NASA by the Smithsonian Astrophysical Observatory.

http://wwwastro.msfc.nasa.gov/xray/axafps.html: Chandra Project Science, at the NASA Marshall Space Flight Center.

http://hea−www.harvard.edu/HRC/: Chandra High−Resolution Camera (HRC) team, at the Smithsonian Astrophysical Observatory (SAO).

http://www.astro.psu.edu/xray/axaf/axaf.html: Advanced CCD Imaging Spectrometer (ACIS) team at the Pennsylvania State University (PSU).

http://acis.mit.edu/: Advanced CCD Imaging Spectrometer (ACIS) team at the Massachusetts Institute of Technology.

http://www.sron.nl/missions/Chandra: Chandra Low−Energy Transmission Grating (LETG) team at the Space Research Institute of the Netherlands.

http://www.ROSAT.mpe−garching.mpg.de/axaf/: Chandra Low−Energy Transmission Grating (LETG) team at the Max−Planck Institut fur extraterrestrische Physik (MPE).

http://space.mit.edu/HETG/: Chandra High−Energy Transmission Grating (HETG) team, at the Massachusetts Institute of Technology.

http://hea−www.harvard.edu/MST/: Chandra Mission Support Team (MST), at the Smithsonian Astrophysical Observatory.

http://ipa.harvard.edu/: Chandra Operations Control Center, operated for NASA by the Smithsonian Astrophysical Observatory.

http://ifkki.kernphysik.uni−kiel.de/soho: EPHIN particle detector.

REFERENCES

[1] See Mendez, M. SPIE, 4851−05 in these proceedings and references therein.
[2] See Flanagan, K. SPIE 4851−04 in these proceedings and references therein.
[3] See Murray, S. S. SPIE 4851−02 in these proceedings and references therein.
[4] See Garmire, G. P. et al. SPIE 4851−03 in these proceedings and references therein.
[5] O'Dell, S. et al. 2003, Proceedings of the SPIE, Volume 4851, pp. 77−88.
[6] Tsuboi, Yohko; Maeda, Yoshitomo; Feigelson, Eric D.; Garmire, Gordon P.; Chartas, George; Mori, Koji; Pravdo, Steven H. 2003, The Astrophysical Journal, Volume 587, Issue 1, pp. L51−L54.
[7] Pictures that are publicly available at the Chandra web site at http://chandra.harvard.edu have credits labeled "Courtesy of". The acronyms may be found at this site.
[8] Gladstone, R. et al. 2002, Nature, Volume 415, pp. 1000−1003.
[9] Elsner, R. F. et al. 2002, The Astrophysical Journal, Volume 572, pp 1077−1082.
[10] Dennerl, K. 2002, Astronomy and Astrophysics, Volume 394, pp.1119−1128.
[11] Dennerl, K. 2002, Astronomy and Astrophysics, Volume 394, pp.1119−1128.
[12] Baganoff, F. K.; Maeda, Y.; Morris, M.; Bautz, M. W.; Brandt, W. N.; Cui, W.; Doty, J. P.; Feigelson, E. D.; Garmire, G. P.; Pravdo, S. H.; Ricker, G. R.; Townsley, L. K., 2003, The Astrophysical Journal, Volume 591, Issue 2, pp. 891−915.
[13] Burrows, D. et al. 2000, The Astrophysical Journal, Volume 543, L149. See also SPIE 4851−03 in these proceedings.
[14] Kaastra, J. S., Mewe, R., Liedahl, D. A., Komossa, S., and Brinkman, A. C. 2000, Astronomy and Astrophysics, Volume 354, L83.
[15] Brinkman, A. C., Kaastra, J. S., van der Meer, R. L. J., Kinkhabwala, A., Behar, E., Paerels, F., Kahn, S. M. and Sako, M. 2002, "The Soft X−Ray Spectrum of NGC 1068 Observed with LETGS on Chandra", Astronomy and Astrophysics, submitted.
[16] Grindlay, J. E., Heinke, C., Edmonds, P. D., and Murray, S. S. 2001, Science, Volume 290, p. 2292.
[17] Fabian, A. C., Sanders, J. S., Ettori, S., Taylor, G. B., Allen, S. W., Crawford, C. S., Iwasawa, K., Johnstone, R. M., and Ogle, P. M. 2000, MNRAS, Volume 318, L65
[18] Markevitch, M.; Gonzalez, A. H.; David, L.; Vikhlinin, A.; Murray, S.; Forman, W.; Jones, C.; Tucker, W. 2002, The Astrophysical Journal, Volume 567, Issue 1, pp. L27−L31.
[19] Markevitch, M.; Ponman, T. J.; Nulsen, P. E. J.; Bautz, M. W.; Burke, D. J.; David, L. P.; Davis, D.; Donnelly, R. H.; Forman, W. R.; Jones, C.; and 12 coauthors 2000, The Astrophysical Journal, Volume 541, Issue 2, pp. 542−549.
[20] See for example the discussion in Fabian, A.C. 2002, "Cooling Flows in Clusters of Galaxies" in Lighthouses of the Universe: The Most Luminous Celestial Objects and Their Use for Cosmology, Proceedings of the MPA/ESO/, p. 24.
[21] Marshall, H. L.; Miller, B. P.; Davis, D. S.; Perlman, E. S.; Wise, M.; Canizares, C. R., and Harris, D.E. 2002; The Astrophysical Journal, Volume 564, pp. 683−687.
[22] Perlman, E. S. et al. 2001, The Astrophysical Journal, Volume 561, Issue 1, pp. L51−L54.
[23] Pavlov, G. G.; Teter, M. A.; Kargaltsev, O.; Sanwal, D. 2003, The Astrophysical Journal, Volume 591, Issue 2, pp. 1157−1171.
[24] Mather, J. C. et al. 1990, The Astrophysical Journal, Volume 354, L4.
[25] Hasinger, G. et al. 1998, Astronomy and Astrophysics, Volume 329, 482.
[26] Alexander, D. M.; Bauer, F. E.; Brandt, W. N.; Hornschemeier, A. E.; Vignali, C.; Garmire, G. P.; Schneider, D. P.; Chartas, G.; Gallagher, S. C. 2003, The Astronomical Journal, Volume 125, Issue 2, pp. 383−397. and references threin.
[27] Giacconi, R., Rosati, P., Tozzi, P., Nonino, M., Hasinger, G., Norman, C., Bergeron, J., Borgani, S., Gilli, R., Gilmozzi, R., Zheng, W. 2001, Astrophysical Journal, Volume 551, 642.